SAE INTERNATIONAL

ARTICLE INFO
Article ID: 14-12-02-0013

doi:10.4271/14-12-02-0013

Influence of Driving Behavior on Thermal and Lifetime Characteristics of Electric Machines for Automotive Applications

Lucas Vincent Hanisch,[1] Sridhar Balasubramanian,[1] Marcel Sander,[2] Markus Henke,[1] Roman Henze,[2] and Ferit Küçükay[3]

[1]Technische Universität Braunschweig, Institute for Electrical Machines, Traction and Drives, Germany
[2]Technische Universität Braunschweig, Institute of Automotive Engineering, Germany
[3]Center for Automotive Engineering in the Innovationsgesellschaft Technische Universität Braunschweig mbH, Germany

Abstract

Increasing stress on power-dense electric traction machines is prompting scientists to intensify investigations into the reliability and lifetime of automotive drives in particular. Special focus is placed on the electrical insulation system, whose probability of failure increases sharply at higher stresses. The influence of physical parameters on the lifetime is investigated in many publications. There is consensus among scientists that high temperature significantly damages the insulation system of electric machines and leads to failures. In this article, the human influence is additionally investigated by considering three different driving behaviors. A mild, an average, and a sporty driver behavior is examined on a highway, a rural, and an urban driving cycle. The driving cycles are used as input to calculate the thermal effects in an initial model. As a further step, a lifetime model is developed on the basis of measured data, which indicates the lifetime as a function of the previously calculated temperature.

History

Received: 11 Apr 2022
Revised: 01 Aug 2022
Accepted: 23 Sep 2022
e-Available: 14 Oct 2022

Keywords

Lifetime modeling, Thermal modeling, Electric vehicle, Electric machines, Insulation system

Citation

Hanisch, L., Balasubramanian, S., Sander, M., Henke, M. et al., "Influence of Driving Behavior on Thermal and Lifetime Characteristics of Electric Machines for Automotive Applications," *SAE Int. J. Elect. Veh.* 12(2):247–261, 2023, doi:10.4271/14-12-02-0013.

ISSN: 2691-3747
e-ISSN: 2691-3755

I. Introduction

To achieve climate targets and expand electromobility, there is a great need for electric traction drives. Developments in the market for electric vehicles and traction drives show that power-dense machines, in particular, offer competitive advantages. Particularly in the luxury segment and in racing, the requirements in terms of space, weight, and performance are enormous. Since the thermal utilization of electric machines limits the performance, research questions concerning the thermal performance of electric machines or thermal management are increasingly being investigated [1, 2]. Since in automotive applications, the electric machine must be considered as part of the entire drivetrain and the overall system has many variable parameters, scalable thermal models are increasingly being developed to represent different machines [3].

With increasing thermal utilization, the automotive industry simultaneously specifies high-reliability requirements, especially in the area of novel electric vehicles. However, high temperatures aid destructive mechanisms such as partial discharges and accelerate the aging of various electric machine components [4]. The reliability of the insulation system of electric machines, which mainly consists of enamel-insulated wires, insulation papers, and impregnating resin, is sensitive to the thermal boundary conditions and therefore plays a critical role in the design of machines with high thermal utilization.

Many publications deal with the reliability and lifetime of electrical insulation systems. In [5], complete stators of electric machines are subjected to thermal cycles and the lifetime is investigated. In [6], stators are also used as test specimens. Compared with [5], different resins and the influence of impregnation processes are additionally investigated here. Since the use of complete stators is very costly, simpler test specimens are often used which represent real machines and allow more general statements to be made. Therefore in [7, 8], thermal investigations are carried out on motorettes that represent low-voltage machines such as those used in electric vehicles. In order to increase the number of test specimens and thus the statistical significance at the same effort, test specimens can be further simplified and only individual components of the insulation system can be considered. Twisted-pair test specimens can be used to perform lifetime tests on hairpin windings [9] or round wire windings [10].

Compared to the majority of publications dealing with the lifetime and thermal stress of electric machines in vehicles, realistic load collectives and driving cycles are additionally considered in this article. Therefore, the presented methodology allows us to investigate the influence of driving behavior on thermals and the lifetime of electric traction machines. An overview of the methodology of this article is presented in Figure 1. Realistic driving cycles, explained in Section II, are used as input. Based on these cycles, a thermal model of the electric machine is created and the winding temperature at each time point is calculated. The thermal model is presented in Section III. The lifetime model is based on a statistical modeling approach. Therefore, lifetime measurements on test specimens are performed next. Using a regression model, the lifetime can then be calculated as a function of temperature, and the individual damages to the electric machine can be accumulated using Miner's rule. The lifetime model is explained in Section IV.

FIGURE 1 Overview of the modeling methodology.

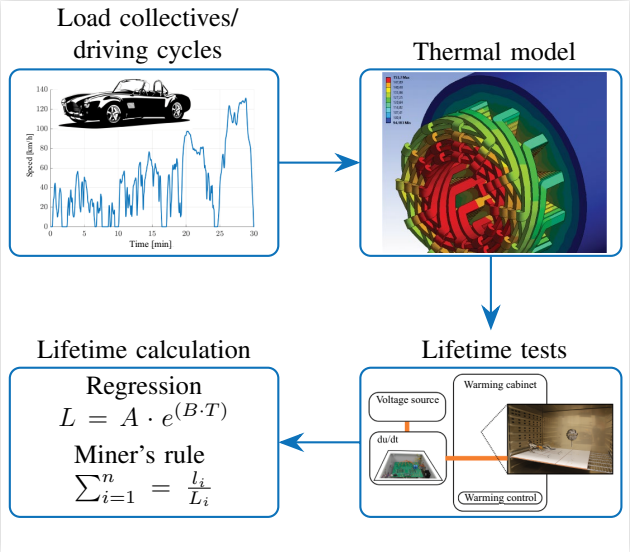

II. Customer Driving Cycles

In order to investigate the thermal effects and lifetime of electric machines in vehicles, information about real vehicle use by customers are required instead of standardized driving cycles such as the WLTP. For this the three-dimensional (3D) Method was developed by Küçükay in [11, 12]. It is an approach to systematically describe the interaction between the driver, driven vehicle, and driving environment. The first application was transmission development, with a focus on lifetime calculation. At the Institute of Automotive Engineering (IAE), the method has since been further developed and was applied on various subjects regarding dimensioning, testing, and calibration of, e.g., power train, chassis, and advanced driver assistance systems. The main element of the 3D Method is the 3D parameter space. For lifetime analysis the parameters driving style (driver), road type (driving environment), and vehicle

load (driven vehicle) have proven to be the most significant. Driving style is divided into three categories: mild, average, and sporty. In the case of road type, a distinction is made between urban, rural, and mountain roads, as well as highways. Vehicle load is divided into light, medium, and full load, as well as full load with trailer.

In this article, the influence of driving style and road type is investigated. Therefore driving cycles for the abovementioned three driving styles and three road types (urban roads, rural roads, and highways) are analyzed. The cycles are results of the MOVE3F simulation environment of the IAE [13, 14, 15, 16]. The MOVE3F simulation environment uses a driver model based on statistics generated from measurement data recorded in customer operation. The statistics include probabilities of various parameters like target speed, holding time of a target speed, and accelerator pedal position. The driver model first chooses a target speed and a corresponding holding time for this speed. In the next step based on the difference between actual and target speed as well as the probabilities, an accelerator pedal position and gradient are determined. A detailed description of the driver model is included in [13]. The accelerator pedal position is then used as input for the vehicle model of MOVE3F. As a result a speed profile is generated besides various other parameters of the drivetrain like rotational speeds, torques, etc. In order to achieve a statistical saturation and thus a representative result, relatively long cycles are generated. For reasons of clarity, Figure 2, therefore, shows only sections of the driving cycles. The figure also shows the average speeds $\overline{v}$ and average accelerations $\bar{a}$ of the entire driving cycles in order to quantify the differences between them.

As the figure shows, usual speed limits are sometimes exceeded, especially by the sporty driver. In the case of urban roads, the relatively high maximum speed is a result of urban highways or inner-city expressways where the maximum permissible speed far exceeds the usual maximum speed in cities. When comparing the average speeds, it is noticeable that the sporty driving style stands out from the average or mild driving style, particularly in the urban cycle, where the average speeds are almost identical. In the rural road and highway cycle, the three average speeds differ more clearly from each other. The average speeds for the mild and sporty driving styles are about 10%-15% below or above the average speed of the average driving style.

The vehicle chosen in this article is an all-electric compact car with an electric machine power of 80 kW. Figure 3 shows the corresponding torque-speed characteristic and the power-speed characteristic. Based on the driving resistances, the load and the machine torque at each operating point can be calculated. The driving cycles are sampled every two seconds, resulting in tens of thousands of operating points per cycle. In addition to the characteristic curves, Figure 3 also compares the operating points of the two most opposite driving cycles

FIGURE 2 Sixty-minute excerpt of the various driving cycles.

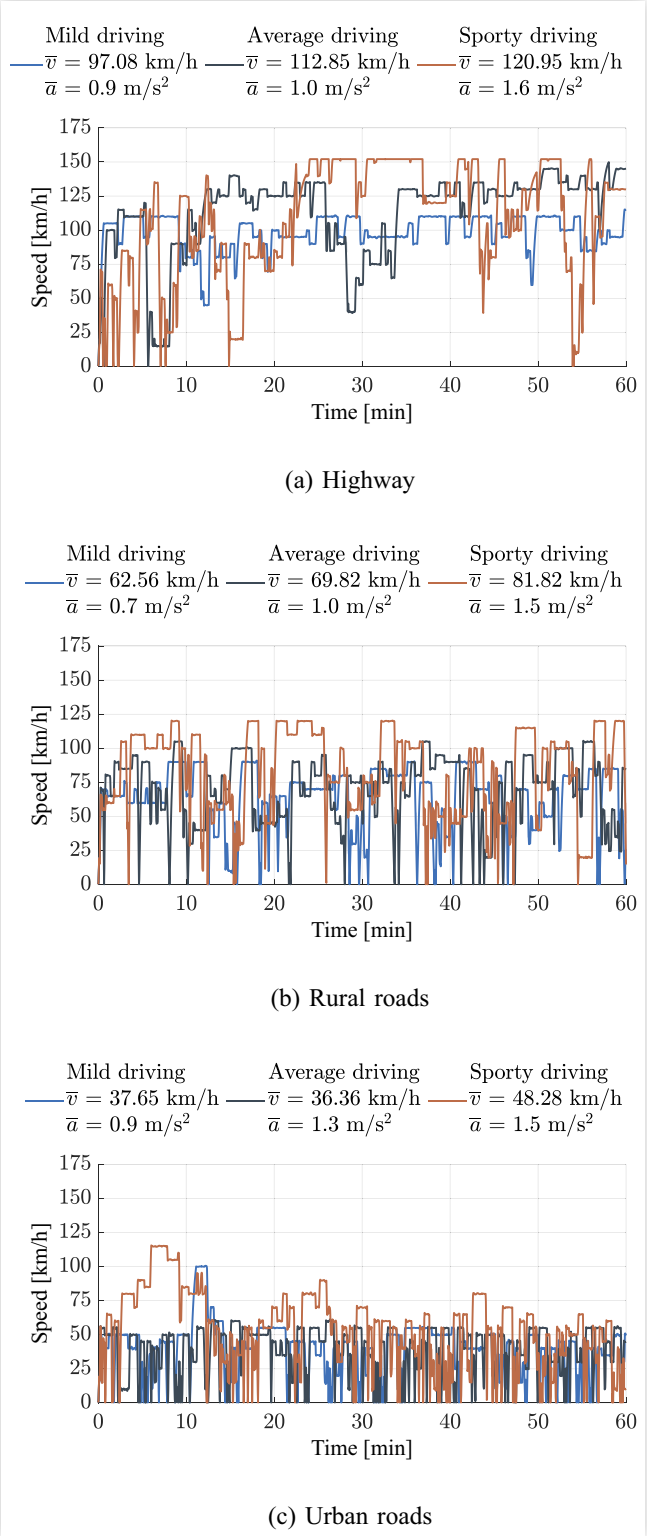

FIGURE 3 Comparison of operating points for sporty highway driving and mild urban driving.

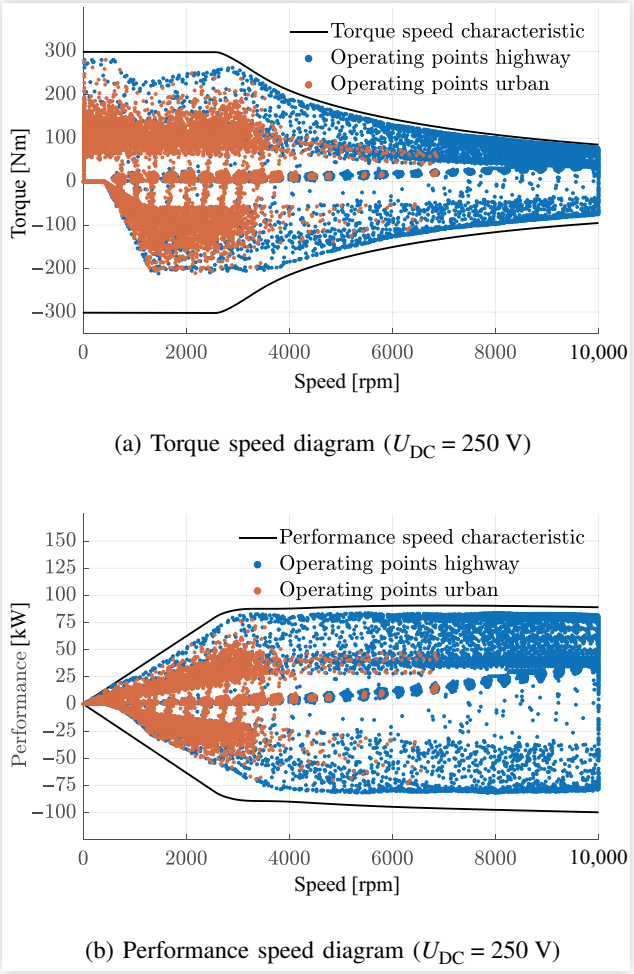

(a) Torque speed diagram (U_{DC} = 250 V)

(b) Performance speed diagram (U_{DC} = 250 V)

(highway and urban roads). The operating points in Figure 3 show how the different driving cycles affect the operation of the electric machine. The electric machine in the urban cycle is predominantly operated at speeds up to 2800 rpm in the partial-load range. On the highway, the machine is predominantly operated at higher speeds in the field weakening region.

The ohmic losses resulting from the d- and q-currents with which the machine is fed at the respective operating points represent a dominant heat source. In the following Section III, the machine model is explained and the temperature distribution in the stator winding of the electric machine during the various driving cycles is presented and analyzed.

III. Thermal Effects on the Electric Machine

In order to investigate the thermal effects due to the driving cycles in Section II, a thermal model of the electric machine is necessary with which the temperature due to the electromagnetic losses

FIGURE 4 Mechanical torque versus speed diagram with stator copper losses ($P_{v,Cu,s}$ at 20°C) contour lines in kilowatts (kW).

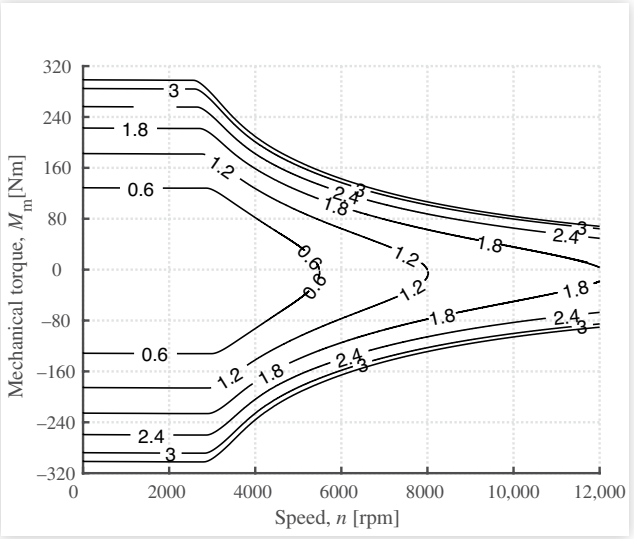

can be calculated. The most important loss sources in a highly utilized inverter-fed electric machine are

- Copper losses in the stator windings including frequency-dependent skin and proximity effects
- Iron losses due to hysteresis and eddy-current effects in laminated iron sheets
- Eddy-currents in the block rotor permanent magnets due to spatial and temporal harmonic field variation
- Bearing friction losses
- Air friction losses on the stator inner bore and the rotor outer surface

The copper, iron, and magnet eddy-current losses constitute the most important loss components and are considered further. The stator windings are made of fine strands of round wires, and therefore, the AC effects can be neglected. Since the iron loss components due to inverter time harmonic currents are difficult to calculate analytically, only the loss component due to fundamental sinusoidal current is considered. The operating points are finely discretized and will be used in combination with the drive cycle requirements in the thermal simulations as shown by the contour maps in Figures 4, 5, and 6.

There are several ways to model the temperature rise in an electric machine, of which the lumped parameter thermal network model and the finite element analysis are the most preferred. One advantage of lumped parameter models is the fast computation time [17]. Finite element analysis, on the other hand, can be used to compute key parameters of the lumped parameter model [18]. In addition, [19] shows that this approach provides realistic results. Heat flow in an electric machine is inherently a 3D problem and a

FIGURE 5 Mechanical torque versus speed diagram with iron losses ($P_{v,Fe}$) contour lines in kilowatts.

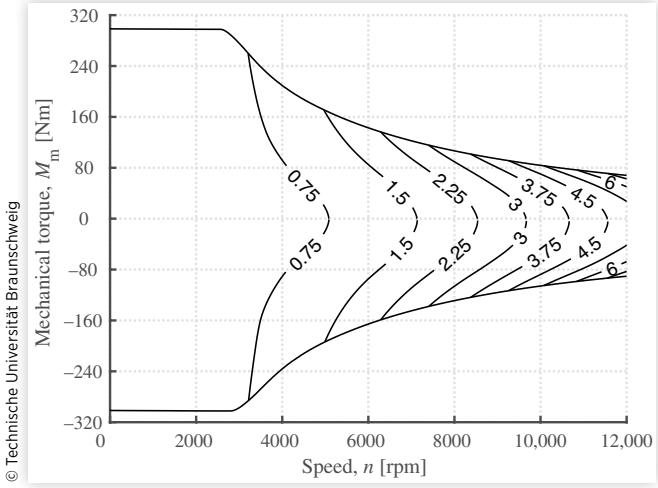

two-dimensional (2D) model order reduction, like in the case of electromagnetic calculations will cause an erroneous result. This is mainly due to the presence of winding overhangs as a heat source and the mixed radial-axial heat flow. However, if the axial heat flow toward the end shields and the bearing housing can be neglected, and if the primary heat sink is the water jacket on the stator outer surface, a 2D finite element model can be used, which reduces the computational time.

The machine is modeled using the software FEMM (Finite Element Method Magnetics). The main features of the model are explained subsequently. All the slot conductors are homogenized along with the resin fill and the insulation paper into

FIGURE 6 Mechanical torque versus speed diagram with rotor permanent magnet eddy-current losses ($P_{v,Ft,M,r}$) contour lines in kilowatts.

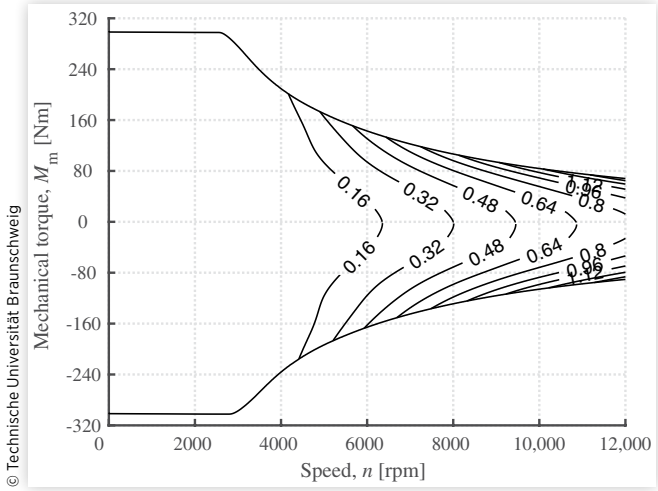

TABLE 1 Assumed material parameters for the thermal simulation.

Material	Thermal conductivity [$Wm^{-1} K^{-1}$]	Sp. thermal capacity [$MJ m^{-3} K^{-1}$]
Copper	380	2.6
Epoxy resin	0.2	0.8
Electrical steel	22	3.54
Permanent magnet	7.6	3.0
Air	0.03	$1.21 \cdot 10^{-3}$

a single material with an equivalent thermal conductivity λ_{E_q} according to Equation 1.

$$\lambda_{E_q} = \lambda_{E_{poxy}} \cdot \frac{(1+k_f)\cdot\lambda_{Cu} + (1-k_f)\cdot\lambda_{E_{poxy}}}{(1-k_f)\cdot\lambda_{Cu} + (1+k_f)\cdot\lambda_{E_{poxy}}} \qquad \text{Eq. (1)}$$

where λ_{Cu} and $\lambda_{E_{poxy}}$ are the thermal conductivities of copper and insulation material and k_f is the copper slot fill factor, which is assumed to be 0.45. The material parameter values used in the simulation are given in Table 1. The validity of this slot homogenization by means of Equation 1 is demonstrated in [14].

Due to the periodicity, only a single magnet pole is sufficient. The heat sources are specified as volume loss density (W/m^3). The coolant inlet temperature is assumed to be 68°C, and the equivalent thermal heat transfer coefficient between the stator outer surface and the water jacket is 3000 $Wm^{-2} K^{-1}$. Once the model is set up, the transient simulations at various time steps are run by taking the inputs from the drive cycle.

The temperature can be evaluated at different machine components at different times. Figure 7 shows the frequency distribution of the temperatures in the stator winding at different driving cycles and different driving behaviors. In addition, the average temperature $\overline{T}$ is given. The highest temperatures and largest absolute temperature differences are seen on the highway cycle. In comparison, the rural cycle has less influence on the temperature distribution and on the urban cycle, especially since the temperatures are very similar in the mild and average driving behavior. The average temperatures here differ by only 2.6°C, while the average temperature for the sporty driving behavior is 92.9°C and about 15% higher than the average temperature for the average driving behavior. In percentage terms, a mild driving behavior on the highway has a particularly strong influence on the temperature of the electric motor. The average temperature here is only 136.4°C, which is more than 20% below the average temperature of the average driving behavior. The opposite behavior can be seen with the rural driving cycle. The sporty driving behavior has a more sensitive effect on the temperature distribution. Compared to the average driving behavior, the average temperature rises by more than 21% to 132.7°C and increases the average temperature more than a mild driving behavior reduces it (only 11.22%). The temperatures in Figure 7 represent the load spectra on the basis of which the lifetime calculation is carried out according to Miner's rule in Subsection IV-D.

FIGURE 7 Histograms of the temperature at different driving behaviors and cycles.

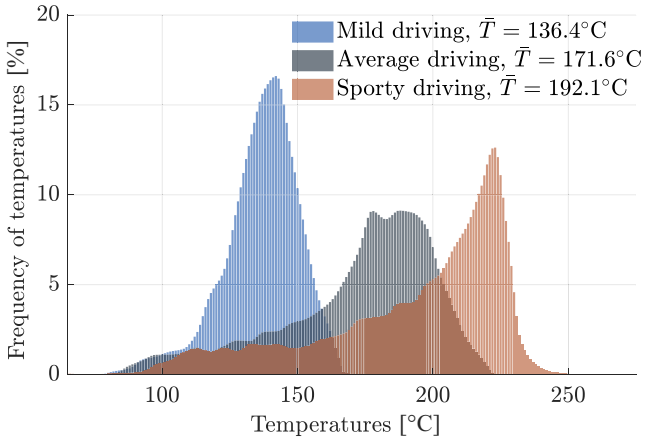

(a) Temperature distribution on the highway

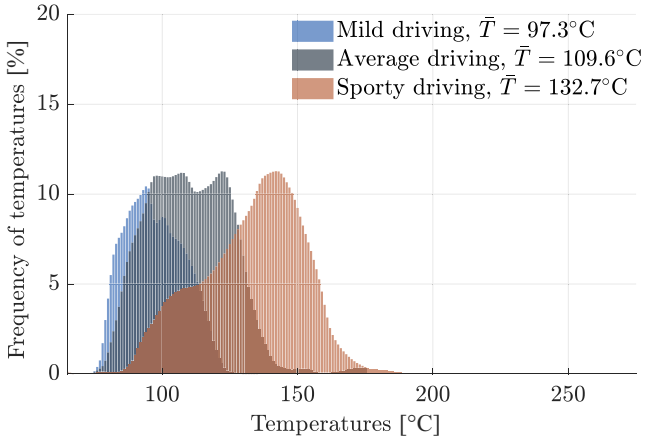

(b) Temperature distribution on the rural roads

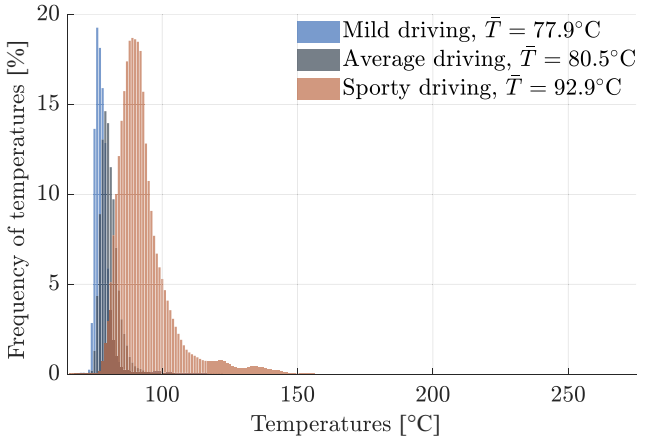

(c) Temperature distribution on the urban roads

An initial comparison of Figures 7 and 20 already shows that higher temperatures lead to lower lifetimes. A more detailed analysis is given in Subsection IV-D.

IV. Lifetime Modeling

When modeling the lifetime, a fundamental distinction is made between physical and statistical modeling approaches. An advantage of statistical approaches is that the model quality and the error are quantifiable so that not only a lifetime can be calculated but also a confidence interval in which the expected lifetime is located with a certain probability [21].

First, Subsection IV-A discusses the test bench that was used to perform the measurements. These measurement data are then statistically analyzed in Subsection IV-B and the underlying distribution is determined. In Subsection IV-C, the regression model is developed. In this process, the parameters of the regression model are calculated to ensure that the model fits the measurement data. In order to determine the lifetime as a function of a transient load spectrum, the model is extended in Subsection IV-D to include Miner's damage accumulation. The load spectrum is divided into partial loads that reduce the lifetime of the electric machine. In Subsection IV-E, the same model is used to compare the lifetime of the electric machine with the lifetime of the mechanical transmission.

A. Test Specimen and Test Setup

As previously mentioned, the stator winding insulation system has become one of the most critical components of the electric machine and is focused on in this article [22]. In contrast to earlier critical components such as rolling bearings and gears, which are primarily stressed by axial and radial forces and whose lifetime is less significantly dependent on temperature, this development will be intensified with future increases in thermal stresses in automotive drives [23]. In Section I, the conflict of objectives between realistic test specimens and the effort involved was already discussed, and various publications were cited, which used different test specimens. In this article, on the one hand, a statistical approach is followed which benefits from a larger sample size, and on the other hand, the stator winding is focused as a critical component, twisted pair test specimens as proposed in the International Electrotechnical Commission (IEC) 60172 standard are used here [24]. As these test specimens are strong simplifications of the real machine, this article does not claim to predict the exact lifetime of the vehicle. However, general statements on temperature behavior, lifetime, and the influence of driving behavior are possible. However, if other test specimens are chosen, the methodology is also suitable for the exact prediction of a lifetime.

An aging test bench was developed to thermally stress the test specimens. The equivalent circuit is shown in Figure 8. The test specimens are located inside a heating chamber, which

FIGURE 8 Diagram of the test bench for thermal stress control of the specimens.

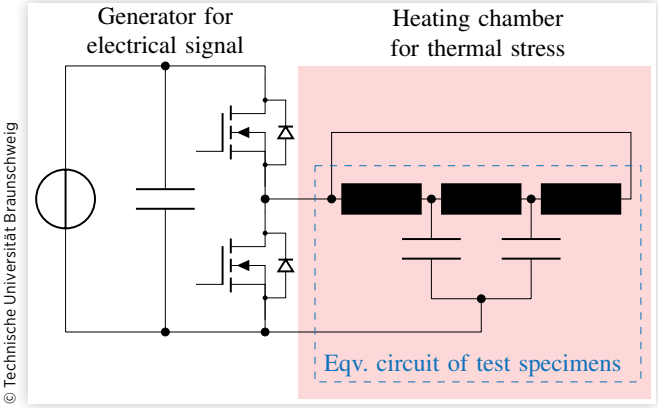

can generate temperatures or temperature cycles up to 300°C. The end of life of a test specimen was defined as insulation failure and the occurrence of electrical breakdown. To measure this breakdown, the test specimens are connected during thermal aging to a half-bridge with two SiC MOSFETs that generate an electrical signal and can simultaneously electrically stress the test specimens for future research studies. As long as the insulation of the test specimen is intact, the test specimen capacitance is charged to the DC link voltage when the top switch of the half-bridge is closed. With the exception of the recharging process of the test specimen capacitance, when the switching state of the half-bridge changes, no current flows when the isolation is intact. If the pulse is switched off afterward, this capacitance discharges again. In the event of an electrical breakdown, a short-circuit current flows through the test specimen causing, among other things, a voltage drop across the semiconductors. In order to immediately switch off the affected half-bridge in the event of a short circuit, a desaturation detection function (DESAT) is used. The DESAT detects the voltage drop and switches off the half-bridge. This overcurrent detection is independent of the drive controller and has a very short response time. If the DESAT detects a failure, the lifetime until the breakdown is stored.

B. Evaluation of the Measurement Results

The necessary measurements to parameterize the lifetime model were carried out at three different temperatures at 175°C, 200°C, and 225°C. The used enameled copper wire has insulation Class F and is thus approved for continuous operation up to 155°C. Accelerated aging cycles beyond the permissible temperature range are necessary to obtain measurement results in an acceptable time and are recommended in the IEC 60034-18-21 standard [25]. According to [25], the three test condition temperatures were deliberately chosen above the temperature of thermal Class F in order to accelerate aging. As a second aging factor, the electrical signal is added, which is described in Subsection IV-A and triggers the DESAT.

FIGURE 9 Histograms of measured failures and normal/Weibull probability density functions (pdf) at different temperatures.

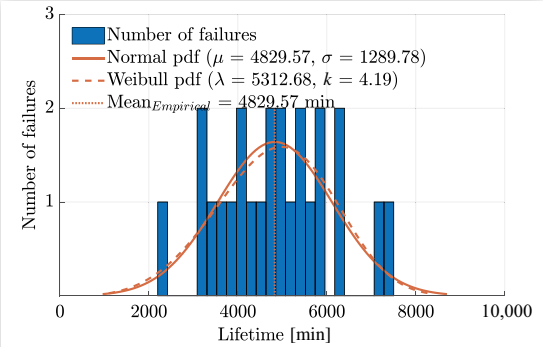

(a) Failures and probability density functions (pdf) at 175°C

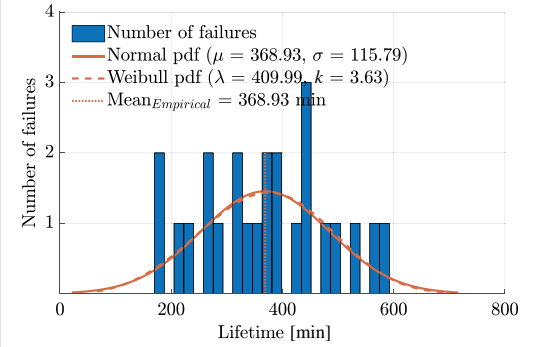

(b) Failures and probability density functions (pdf) at 200°C

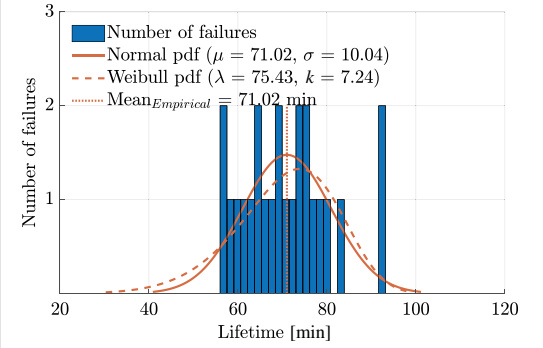

(c) Failures and probability density functions (pdf) at 225°C

The simultaneous electrical and thermal stress was implemented in order to be able to extend the lifetime model in the future to include electrical parameters and to investigate interactions between electrical and thermal parameters. The additional electrical aging is generated by a voltage amplitude of 400 V and a clock frequency of 20 kHz. The high temperatures of 175°C, 200°C, and 225°C ensure that the aging is primarily due to thermals. The measurement results at the different temperatures are shown in the histograms in Figure 9. The different lifetimes show the influence of temperature on the

lifetime. First, the measurement results at the three temperatures are analyzed independently. The system noise can be assessed on the basis of various statistical parameters. The knowledge about the noise in the system is necessary to evaluate whether a temperature change has a statistically significant influence on the lifetime of the stator winding of the machine, or whether the influence is probably smaller than the noise and thus cannot be evaluated. In addition, the distribution of the measured values is investigated.

The two-parameter Weibull distribution is a statistical distribution that is often used for modeling failure rates of accelerated lifetime tests [27, 26]. The Weibull distribution function of the lifetime L as a function of the temperature T is described in Equation 2.

$$L(T) = 1 - e^{-\left(\frac{T}{\lambda}\right)^k} \qquad \text{Eq. (2)}$$

The Weibull distribution is described by the scale parameter λ and the shape parameter k. The scale parameter λ is also referred to as the characteristic lifetime and, in lifetime analyses, is the time period after which approximately 63.2% of the test specimen have failed. Figures 9(a), 9(b), and 9(c) show the scale and shape parameters of the corresponding Weibull distributions estimated using the maximum likelihood method. Another distribution that describes the measurement results similarly well is the normal distribution. The probability density functions of the normal distribution are also shown in Figures 9(a), 9(b), and 9(c). They are described by the mean value μ, and the standard deviation σ. The probability density functions at 175°C and 200°C are very similar, but they differ more at 225°C. In the plots from Figure 9, the empirical mean value is additionally marked by a vertical line.

The standard deviations of the normal distributions from Figures 9(a), 9(b), and 9(c) correspond to the empirical standard deviation and characterize the system noise. The measurements show a rather high experimental scatter. The high scatter of twisted pair test specimens in thermal aging tests is a known problem and was investigated and compared with other test specimens in [28]. In order to be able to better compare the scatter of the three tests, the coefficient of variation C_{var} can be used as a statistical parameter. It relates the standard deviation σ to the mean value $\mu\left(C_{var} = \frac{\sigma}{\mu}\right)$. In addition to the coefficient of variation C_{var}, further statistical parameters are given in Table 2.

Skewness describes the degree of asymmetry around the mean of the data points. The normal distribution has a skewness of 0 and is distributed perfectly symmetrically around the mean. A negative value indicates that the distribution is skewed to the left of the symmetric distribution, and a positive value indicates skewness to the right of the symmetric distribution. With a z-standardized skewness of ±1.96, a normal distribution can be assumed. The kurtosis shows how peaked the data are, whereas the normal distribution has a kurtosis of 0. With a negative kurtosis, the data are flatter, and with a positive kurtosis, the data are more peaked than with the normal distribution.

Two other statistical parameters are suitable for examining the measurement data for a specific distribution. The Kolmogorov-Smirnov test and the Akaike information criterion (AIC). The Kolmogorov-Smirnov test compares the deviation of the observed distribution function with a theoretical distribution function. High p-values indicate a good agreement between the distributions. The strength of the AIC lies in the comparison of two distributions because it describes how much more likely one of the two distributions is. The objective is to minimize the AIC value. The AIC is calculated from the maximum value of the likelihood function $\hat{L}_{AIC}$ and the number of parameters n_{AIC} (3).

$$AIC = 2n_{AIC} - 2\ln\left(\hat{L}_{AIC}\right) \qquad \text{Eq. (3)}$$

A comparison of the statistical values from Table 2 shows a slight tendency toward normally distributed data. However, neither of the two distributions can be significantly excluded. The QQ plots in Figure 10 are the last indication of normal distribution. In this diagram, the quantiles of the measured data and the deviation from the ideal normal or Weibull distribution are shown. In summary, it can be stated that due to the high coefficient of variation of the measurement results, no reliable statement regarding distribution can be made on

TABLE 2 Summary of statistical parameters.

$Feature_{empirical}$	T = 175°C	T = 200°C	T = 225°C
Lifetime mean [min]	4829.57	368.93	71.02
Standard deviation	1289.78	115.79	10.04
Coeff. of variation [%]	26.71	31.39	14.14
Skewness (z-standardized)	0.384	0.202	1.173
Kurtosis (z-standardized)	2.573	2.157	2.924
$Feature_{normal}$	T = 175°C	T = 200°C	T = 225°C
Kolmogorov-Smirnov (p-value)	1.000	0.998	0.992
Akaike information criterion	412.87	297.18	179.82
$Feature_{weibull}$	T = 175°C	T = 200°C	T = 225°C
Kolmogorov-Smirnov (p-value)	0.999	0.998	0.838
Akaike information criterion	413.11	296.69	183.29

the basis of the histograms in Figure 9 alone. The statistical parameters in Table 2 confirm this because the values for the Kolmogorov-Smirnov test and the AIC are similar for the normal distribution and Weibull distribution. Finally, the QQ plots in Figure 10 provide information about the distribution to be assumed here. Figure 10 shows that the difference of the measured values from the normal distribution is smaller than from the Weibull distribution. Especially in the upper quantiles, the measurement results differ strongly from the Weibull distribution, while the normal distribution shows better agreement with the measurements. Unlike in many other papers, the argument here is not with the Weibull but with the normal distribution.

FIGURE 10 QQ plots of measurement data versus normal and Weibull distribution.

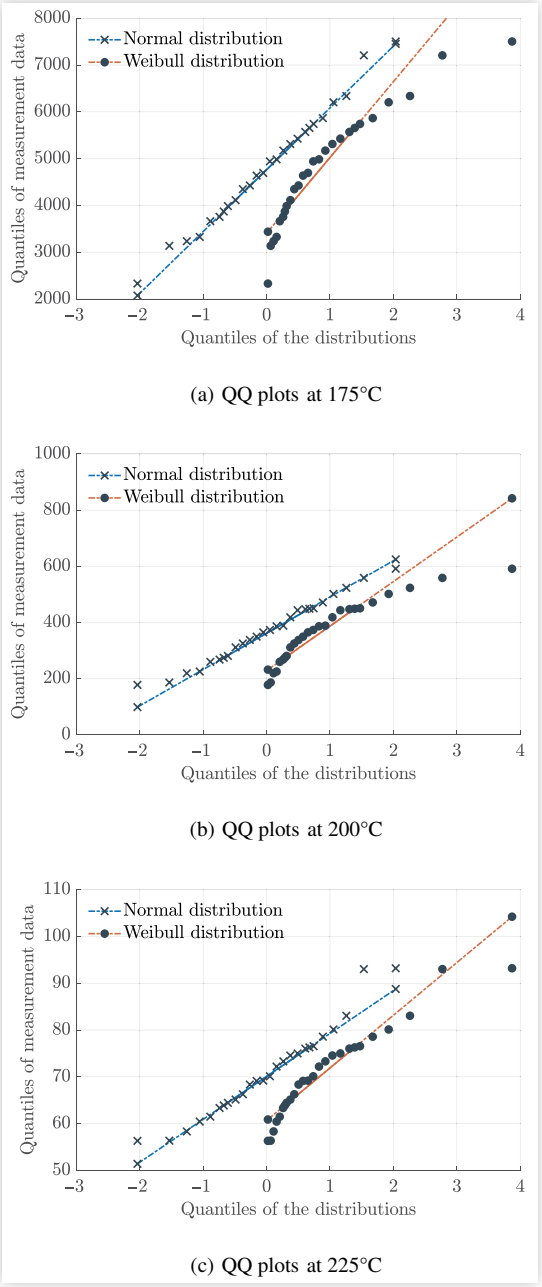

(a) QQ plots at 175°C

(b) QQ plots at 200°C

(c) QQ plots at 225°C

C. Linear Regression and Lifetime Modeling

Similar to the QQ plots in Figure 10 where the quantiles of the measured values are plotted versus the quantiles of the normal and Weibull distributions, respectively, the distribution of the residuals, i.e., the difference between the actual measured lifetime values and the lifetime predicted by the model, should also be investigated. It is desirable that the residuals of the regression model do not show a distinct pattern but are randomly distributed and follow a normal distribution. Normally distributed residuals lead to an optimal calculation of the significance level and confidence intervals when developing regression models. Two key parameters with which the quality and uncertainty of the regression model can be quantified.

Figure 11 shows residual probability plots for six different transformations. Transforming data, in this case the lifetime measurements, is a common method in regression analysis to improve model fit. Fully normally distributed residuals would follow the blue lines in Figure 11. The bottom left graph in Figure 11 shows the residual probability plot of the untransformed lifetime measurements. The uneven distribution of the residuals and the two steps indicate an inadequate model. The steps can occur, for example, if the measurement results are influenced by an additional variable besides temperature, which is not considered here. A comparison of the plots in

FIGURE 11 Studentized residual probability plots of different transformations to analyze whether the residuals are normally distributed.

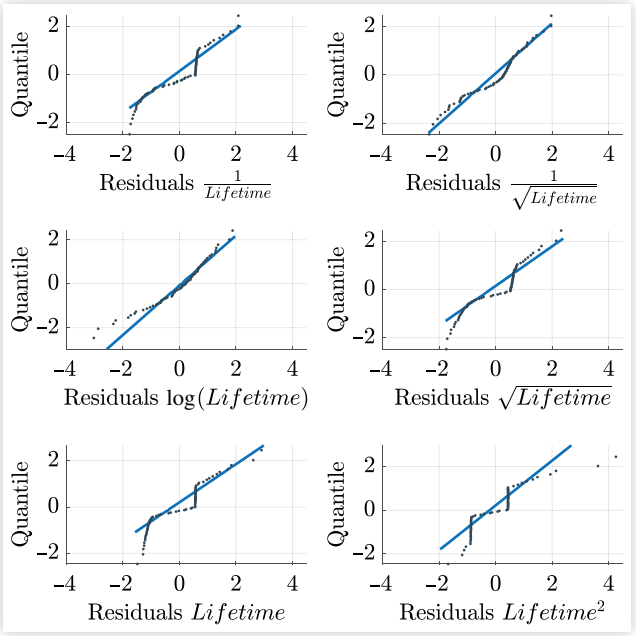

Figure 11 shows that the residuals tend to follow a normal distribution after a logarithmic or a reciprocal square root transformation. After logarithmic transformation, the residuals follow the normal distribution very well. However, heavy tails can be seen at the lower end and light tails at the upper end. The light tails at the upper end are not a problem because they show that the extreme residuals are smaller than expected. This leads to the fact that the calculation of the confidence intervals is rather conservative. A calculated 95% confidence interval could turn out to be a 98% confidence interval in reality. The heavy tails for the negative residuals are somewhat more pronounced and indicate a slightly left skew of the distribution. If the residuals are larger than expected, this tends to lead to a more optimistic calculation of the confidence intervals. A calculated 95% confidence interval could in reality also correspond to a 92% confidence interval. This has to be taken into account when evaluating the regression model.

To evaluate which transformation optimizes the model fit best, a Box-Cox transformation plot as shown in Figure 12 is also suitable. The Box-Cox transformation searches for a suitable exponent k with which to power the measurement data y so that the error term of the regression model is reduced. The power of zero corresponds to a logarithmization of the measurement data y. Equation 4 shows the Box-Cox transformation of the measurement data y

$$y(k)=\begin{cases} y^k & \text{if} \quad k\neq 0 \\ \log(y) & \text{if} \quad k=0 \end{cases}. \qquad \text{Eq. (4)}$$

The Box-Cox plot in Figure 12 shows the residual sums of squares (the error term) on the vertical axis for the six transformations, which were also used for the residual probability plots in Figure 11. As already expected, the measurement data after the logarithmic and reciprocal square root transformation, whose residuals in Figure 11 most resembled a normal distribution, also show the lowest error terms in the Box-Cox diagram. Compared to Figure 11, the choice of the transformation of the measurement data based on the results in Figure 12 clearly falls on a logarithmic transformation due to the lowest error term.

The good data fit after logarithmic transformation also makes sense from a physical point of view since Arrhenius and Dakin already recognized an exponential relationship between the lifetime or chemical reaction rates and the temperature, and a logarithmic transformation leads to the linearization of exponential relationships [29]. The transformed measurement data can therefore be described well with a simple linear function and are similar to Dakin's model:

$$\ln\big(L(T)\big)=\ln(A)+B\cdot T. \qquad \text{Eq. (5)}$$

Figure 13 shows the measurement results in box plots and the logarithmic regression model in gray. The regression model with the values of parameters A and B was calculated using the least squares method. In addition, statistical parameters are given to assess the goodness of fit of the regression models. Compared to the R-square, the adjusted R-square takes into account the number of terms in the regression model and increases only if the new term improves the model more than would be expected by chance. This prevents nonsensical functions that statistically represent the measured values very well, but ignore the real physical relationship. RMS means the root mean square.

For better visualization of the measured values, a slight jitter has been inserted in Figure 13. However, as can be seen in Figure 9, the 24 measured data points were measured at constant temperatures. Statistical parameters can also be found in the box plot. The top and bottom bars indicate the maximum and minimum, respectively. The bottom and top of each box indicate the upper and lower quartiles, and the middle bars indicate the medians of the samples.

Compared to the linear model in Equation 5, a reciprocal model can also be used to describe the measured data:

$$\ln\big(L(T)\big)=\ln(a)+\frac{b}{T}. \qquad \text{Eq. (6)}$$

FIGURE 12 Box-Cox transformations to reduce error term and enable better fit.

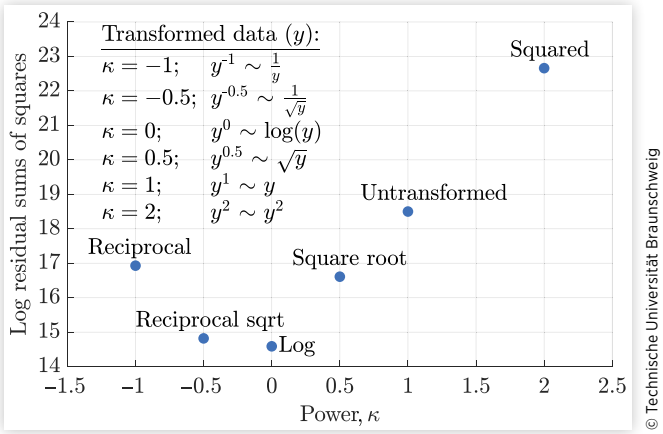

FIGURE 13 Box plot of the measurement points, logarithmic, and Dakin's regression model.

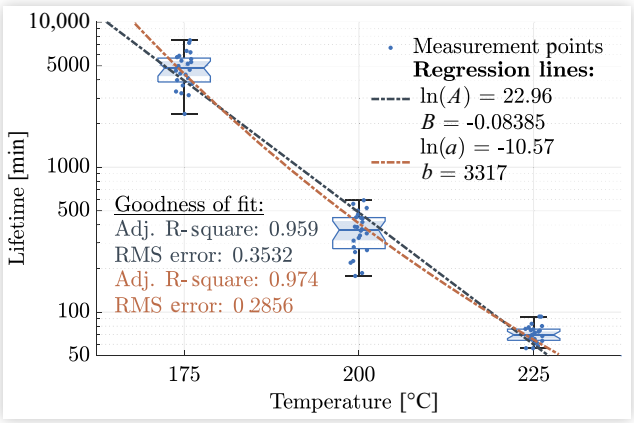

Equation 6 now describes Dakin's exact model and is shown in orange in Figure 13. Although most papers dealing with lifetime modeling use the popular model of Arrhenius and Dakin, criticism of this model should also be pointed out here. In [30], for example, the model from Equation 5 is used because it reproduced the measured data on the lifetime of polymers as a function of temperature better than the model of Arrhenius and Dakin. The two main points of criticism are that the model of Arrhenius and Dakin is only valid for high temperatures and that several chemical reactions take place at the same time and have different effects so the reciprocal model should not be used imprudently. Since the model of Arrhenius and Dakin gives a slightly better data fit and has been verified in many publications, the lifetime model in this article is also based on Equation 6.

D. Lifetime Calculation with Miner's Rule

The regression model can now be used to determine the lifetime at a constant temperature. However, it can be seen from Figures 2, 3, and 7 that electric machines for automotive applications in particular are subjected to a wide load spectrum with different operating points. The lifetime model developed in this article is intended to calculate the remaining lifetime or the percentage lifetime loss after a certain load spectrum, which is represented by the different driving cycles shown in Figure 2. Miner's rule is suitable for this purpose. Here, the duration that the electric machine remains in an operating point l_i is set in relation to the total lifetime in this operating point L_i and the operating points of the load spectrum n are summed up:

$$1-\sum_{i=1}^{n}\frac{l_i}{L_i}=1-\frac{l_1}{L_1}-\cdots-\frac{l_n}{L_n}. \qquad \text{Eq. (7)}$$

The result of Equation 7 is the percentage remaining lifetime of the electric machine. Figure 14 shows the results of the lifetime model for the three different driving cycles for the three driving behaviors. A decreasing lifetime account can be seen on the vertical axis. The horizontal axis shows the range normalized to the average driving behavior. The normalized representation was chosen because this article examines the influence of driving behavior on lifetime and therefore compares driving cycles. It makes less sense to give absolute values in hours or range in kilometers as these would be subject to assumptions. On the one hand, twisted pair specimens according to the IEC 60172 standard are used. Subsection IV-A describes the conflict in the selection and choice of test specimens in more detail, and Section I references publications that use different test specimens. If the research objective were to determine the exact lifetime or range of a particular electric machine, entire stators, drivetrains, or even vehicles would be more appropriate instead of twisted pair specimens. The methodological approach would be the same. First, the purpose of this article is to present the

FIGURE 14 Reduction of the lifetime at different driving behaviors and cycles.

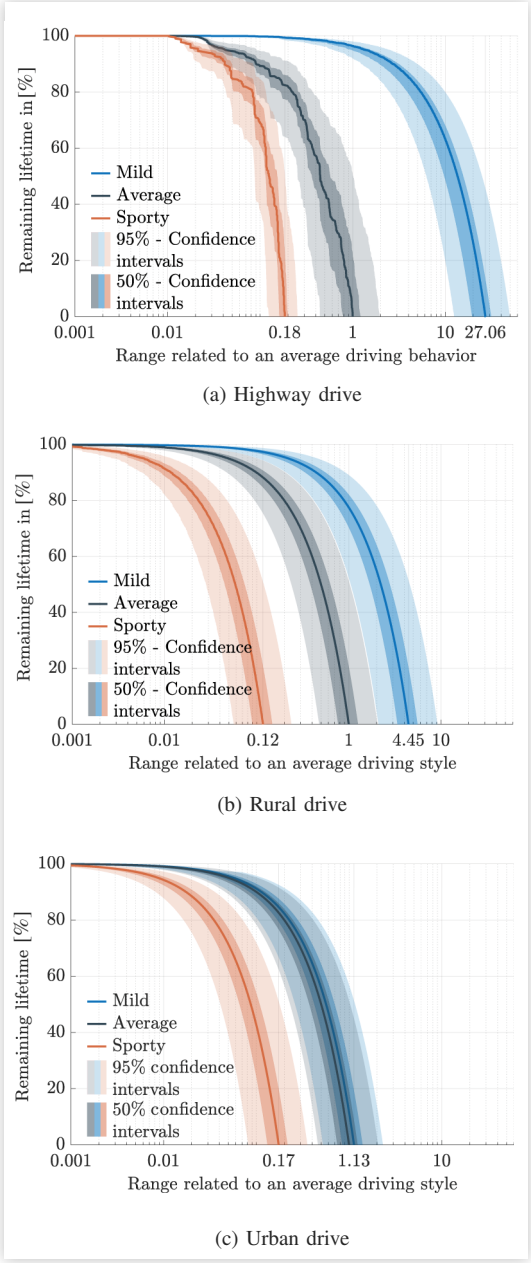

scientific approach and to determine whether the driving behavior influences the thermals and lifetime of an electric machine and how significant this influence is. Second, the thermal degradation process of the insulation system is focused as this has been identified as the weakest point. As mentioned earlier, there are other electrical, chemical, or mechanical degradation processes that affect the lifetime of electric machines and are not considered here. Consideration of electrical degradation mechanisms is planned for the future and has already been considered in the test bench.

In the plots in Figures 14(a), 14(b), and 14(c), the influence of driving behavior on the lifetime of the electric machine on

the highway, rural, and urban roads can be determined. The solid lines indicate the expected lifetime consumption. An advantage of statistical models is that the model quality is quantifiable and robust results can be given. In addition to the expected lifetime, the probability of failure can also be calculated by specifying the standard deviation or confidence intervals. The light and dark transparent areas around the expected lifetime curves show the 95% and 50% confidence interval. Regardless of the driving cycle, it is evident that sporty driving behavior massively reduces the lifetime of the machine and, thus, the range of the vehicle. Compared with the average driving behavior, on the other hand, it can be seen that the mild driving behavior on the highway and rural road has a positive effect on lifetime. Only in urban traffic do the confidence intervals for the average and mild driving behaviors overlap, so no significant influence can be detected here. It is noticeable that the lines in Figure 14(a) for the sporty and average driving styles are not as smooth as in the other figures. The reason for this is the normalization of the range, which is described in the second paragraph of this subsection and enables a clear comparison of the driving cycles. Compared to the sporty and average driving styles on the highway, the absolute ranges for the other cycles are longer so the influence of individual time intervals is low and the curves are displayed more smoothly. The results from Figure 14 are consistent with the calculated temperatures in Figure 7. In Figure 7(c), it can be seen that the mean winding temperature of the machine differs by only 2.6°C for the average and mild driving behavior in the urban drive. In addition, due to the exponential relationship between the lifetime of electric machines and temperature, lower temperatures are less significant than higher temperatures, such as those that occur on the highway. A closer look at the driving behavior in the urban drive [Figure 2(c)] shows that the mean speed for mild driving behavior is even higher than for average driving. This shows that the driving behaviors are very similar here and that there is therefore no significant influence on the lifetime of the electric machine.

E. Lifetime Comparison between the Electric Machine and the Transmission

The lifetime of the entire drivetrain of electric vehicles is not only determined by the electric machine. A comparison with the lifetime of transmissions is intended to show that driving behavior can have different effects on different components and that conflicting goals can arise.

The lifetime of drivetrain components such as transmissions and driveshafts depends on the mechanical stress induced by the torque of the propulsion machines. A common approach to determine the lifetime is the use of the stress-life method and Palmgren-Miner cumulative damage rule (Palmgren-Miner rule). To compare the influence of parameters unrelated to the design of the components, like driving behavior, on lifetime, it is possible to use torque instead of stress. Moreover, synthetic stress-life (S-N) curves can replace the real S-N curves of a component derived from a test on the specimen. In this case the S-N curve up to the number of cycles of fatigue limit N_{FL} (area of high-cycle fatigue) is defined by

$$N_i = N_{FL} \cdot \left(\frac{T_i}{T_{FL}} \right)^{-k}. \qquad \text{Eq. (8)}$$

In Equation 8, T_{FL} is the torque at the fatigue limit, N_i number of cycles at a torque T_i, and k the Wohler exponent, which represents the gradient of the S-N curve in a double logarithmic diagram. For the fatigue limit, different approaches for the S-N curve exist. In this article, the elementary Palmgren-Miner rule is used, which assumes that a fatigue limit does not exist and any stress increases fatigue. In analogy with Equation 7, the remaining lifetime is a result of the number of rotations at a certain torque level n, and the maximum number of rotations at this torque N_i form Equation 8:

$$1 - \sum_{i=1}^{n} \frac{n_i}{N_i} = 1 - \frac{n_1}{N_1} - \cdots - \frac{n_n}{N_n} \qquad \text{Eq. (9)}$$

As a result, a lifetime account similar to Figure 14 can be calculated. Figure 15 shows the lifetime account for the transmission in the nine cycles normalized to the average driving behavior. A Wohler exponent of $k = 7$ was used. The influence of driving style is the same as described before for the electric machine. Compared to the average driving style, a sporty driving style results in higher fatigue and shorter lifetime, whereas a mild driving style has a higher lifetime. However, on highway and urban roads, the influence of driving style on the lifetime is different between the electric machine [Figures 14(a) and 14(c)] and transmission [Figures 15(a) and 15(c)]. As described before, the lifetime of the electric machine of mild drivers on a highway is significantly higher than average drivers; whereas on urban roads, the difference is small. In contrast, the lifetime of the transmission of mild drivers on urban roads is significantly higher than average drivers and relatively small on highways. Due to the lower driving speeds on urban roads, the electric machine is operated at lower speeds and higher torque is available [cf. Figure 3(a)]. In conjunction with more frequent acceleration maneuvers, these torques are used more frequently and lead to higher fatigue of the transmission.

The entire drivetrain is only as reliable as its weakest component. Many studies therefore attempt to identify the most fault-prone component and increase its reliability. In [31], the fault tree model is used so the failure of the electric controller or electric machine leads to the failure of the electric drive system and finally to the failure of the vehicle. The comparison of Figures 14 and 15 shows that the reliability of the individual components, and thus, also the overall reliability of the electric vehicle is additionally influenced by driving behavior. A driver with a mild driving style puts much

FIGURE 15 Reduction of the lifetime of the transmission at different driving behaviors and cycles.

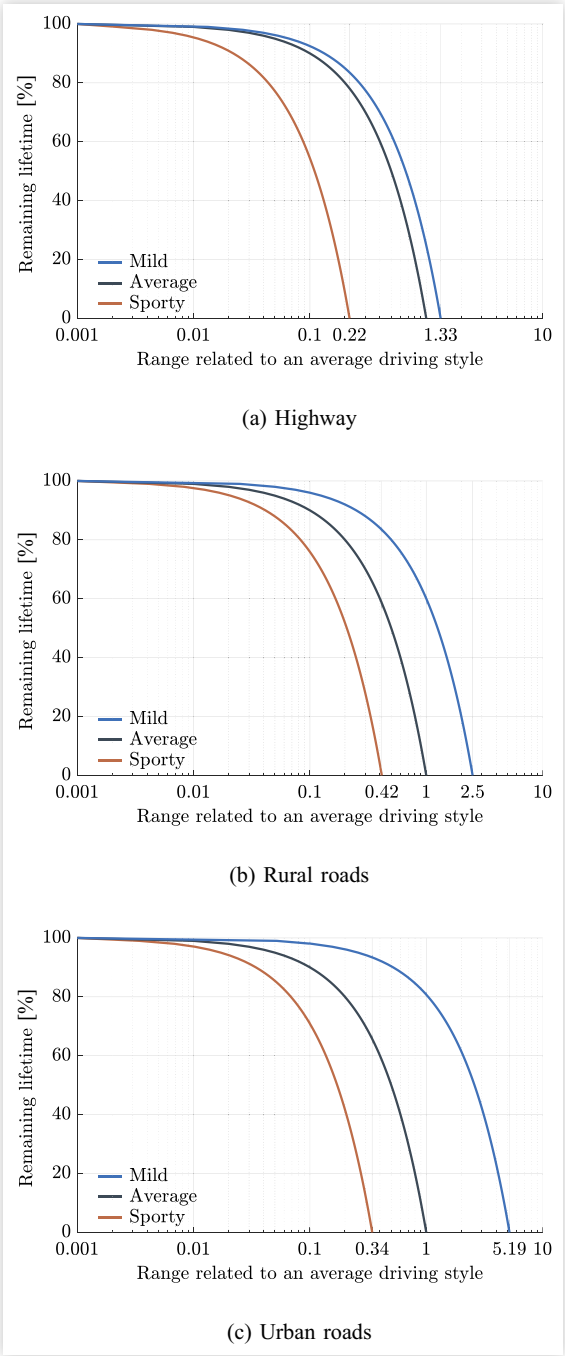

less stress on the electric machine during highway driving compared to average or sporty drivers. The stress on the transmission, on the other hand, is reduced to a lesser extent compared to an average driver. In urban driving, this is reversed. The mild driver puts significantly less stress on the transmission compared to the average or sporty driver. In contrast, the reduction of stress on the electric machine compared to the average driver is very low.

V. Conclusion and Outlook

To investigate the influence of driving behavior on the thermal and lifetime of the electric machine of a compact car, three different driving behaviors (mild, average, sporty) were selected on three different driving cycles (highway, rural road, urban road). First, a thermal machine model was developed and the temperature distribution was calculated as a function of the driving cycles. The lifetime model is based on real measurements carried out by means of twisted pair test specimens at three different temperatures (175°C, 200°C, 225°C). After a detailed examination of the measurement results, a normal distribution was assumed and a logarithmic transformation was performed to increase the data fit. In the subsequent regression model, a simple exponential model and the antiproportional exponential model of Arrhenius and Darkin were reviewed. The latter showed a better fit to the measured data and was selected. Finally, Miner's rule was used to calculate the lifetime at different load collectives. On the highway drive and rural road drive cycles, a significant influence of the driving behavior on the lifetime of the electric machine in the vehicle was shown. Particularly on the highway, the mild driving behavior extends the lifetime of the electric motor by a factor of 27 on average compared to the average driving behavior. In urban traffic, only the sporty driving behavior significantly reduces the lifetime compared to the average driving behavior. The mild driving behavior did not result in any significant difference in the lifetime compared to the average driving behavior. Since transmission lifetime is influenced by high torques, an opposite result is seen here. Although a sporty driving behavior generally reduces the lifetime here as well compared to the average and mild driving behavior, the influence of a mild driving behavior on highways, in particular, has less of an effect on the transmission lifetime than on the lifetime of the electric machine. The transmission lifetime only increases by a factor of 1.33 with mild driving behavior. The reason for this is that high temperatures occur in the machine, but the machine is operated in the field weakening range at low torques.

In future research activities additional damage mechanisms shall be considered. Especially electrical damage mechanisms based on high voltages and fast switching frequencies shall be investigated. Furthermore, the consideration of coupling effects and interactions between the different damage mechanisms could expand the current lifetime model in this article. Additional thermal lifetime measurements at lower temperatures could specify the current model and give precise information about the extrapolation ability.

Contact Information

Lucas Vincent Hanisch
Hans-Sommer-Straße 66
38106 Braunschweig
Germany
l-v.hanisch@tu-braunschweig.de
phone: +495313913906

References

1. Nishanth, F., Johnson, M., and Severson, E.L., "A Review of Thermal Analysis and Management of Power Dense Electric Machines," in *2021 IEEE International Electric Machines & Drives Conference (IEMDC)*, Hartford, CT, 2021, 1-8, doi:10.1109/IEMDC47953.2021.9449520.
2. Soualmi, A., Zidat, F., Lombard, P., and Mokhtari, N., "Thermal Study Comparison of Permanent Magnets Machines Using Finite Element Method (FEM) Electric Vehicles Application," in *2018 21st International Conference on Electrical Machines and Systems (ICEMS)*, Jeju, Korea, 2018, 5964, doi:10.23919/ICEMS.2018.8549302.
3. Pauli, F., Ruf, A., and Hameyer, K., "Thermal Overload Capability of Permanent Magnet Synchronous Motors Employing Scaling Laws," in *2018 XIII International Conference on Electrical Machines (ICEM)*, Alexandroupoli, Greece, 2018, 433-439, doi:10.1109/ICELMACH.2018.8506826.
4. Hanisch, L.V., Dietrich, T.-H., and Henke, M., "Analysis of Partial Discharges and Failure Mechanism in Electrical Machines with Hairpin Winding," in *2021 IEEE 13th International Symposium on Diagnostics for Electrical Machines, Power Electronics and Drives (SDEMPED)*, Dallas, TX, 2021, 1-7, doi:10.1109/SDEMPED51010.2021.9605500.
5. Griffo, A., Tsyokhla, I., and Wang, J., "Lifetime of Machines Undergoing Thermal Cycling Stress," in *2019 IEEE Energy Conversion Congress and Exposition (ECCE)*, Baltimore, MD, 2019, 3831-3836, doi:10.1109/ECCE.2019.8913216.
6. Richnow, J., Stenzel, P., Renner, A., Gerling, D. et al., "Influence of Different Impregnation Methods and Resins on Thermal Behavior and Lifetime of Electrical Stators," in *2014 4th International Electric Drives Production Conference (EDPC)*, Nuremberg, Germany, 2014, 1-7, doi:10.1109/EDPC.2014.6984406.
7. Madonna, V., Giangrande, P., and Galea, M., "Influence of Thermal Aging on the Winding Thermal Conductivity in Low Voltage Electrical Machines," in *2020 23rd International Conference on Electrical Machines and Systems (ICEMS)*, Hamamatsu, Japan, 2020, 123-128, doi:10.23919/ICEMS50442.2020.9291167.
8. Madonna, V., Giangrande, P., and Galea, M., "Influence of Insulation Thermal Aging on the Temperature Assessment in Electrical Machines," *IEEE Transactions on Energy Conversion* 36, no. 1 (2021): 456-467, doi:10.1109/TEC.2020.3001053.
9. Mancinelli, P., Stagnitta, S., and Cavallini, A., "Lifetime Analysis of an Automotive Electrical Motor with Hairpin Wound Stator," in *2016 IEEE Conference on Electrical Insulation and Dielectric Phenomena (CEIDP)*, Toronto, ON, Canada, 2016, 877-880, doi:10.1109/CEIDP.2016.7785538.
10. Moghadam, D.E., Herold, C., and Zbinden, R., "Effects of Resins on Partial Discharge Activity and Lifetime of Insulation Systems Used in eDrive Motors and Automotive Industries," in *2020 IEEE Electrical Insulation Conference (EIC)*, Knoxville, TN, 2020, 221-224, doi:10.1109/EIC47619.2020.9158737.
11. Küçükay, F., "Rechnergestutzte Getriebedimensionierung mit repräsentativen Lastkollektiven," *ATZ - Automobiltechnische Zeitschrift* 92 (1990): 328-333.
12. Küçükay, F., "Repräsentative Erprobungsmethoden in der Pkw-Getriebeentwicklung," *VDI-Berichte* 1175 (1995): 49-65.
13. Müller-Kose, J.-P., "Repräsentative Lastkollektive für Fahrzeuggetriebe," Dissertation, Technische Universität Braunschweig, 2002.
14. Kassel, T., "Optimale Gangzahl für Schaltkollektive für Fahrzeuggetriebe," Dissertation, Technische Universität Braunschweig, 2009.
15. Fugel, M., "Parallele Hybridantriebe im Kundenbetrieb," Dissertation, Technische Universität Braunschweig, 2010.
16. Werra, M., Sturm, A., and Küçükay, F., "Optimal and Prototype Dimensioning of 48V P0+P4 Hybrid Drivetrains," *Automotive and Engine Technology* 5 (2020): 173-186, doi:10.1007/s41104-020-00071-0.
17. Acquaviva, A., Wallmark, O., Grunditz, E.A., Lundmark, S.T. et al., "Computationally Efficient Modeling of Electrical Machines with Cooling Jacket," *IEEE Transactions on Transportation Electrification* 5, no. 3 (2019): 618-629, doi:10.1109/TTE.2019.2936122.
18. Nategh, S., Zhang, H., Wallmark, O., Boglietti, A. et al., "Transient Thermal Modeling and Analysis of Railway Traction Motors," *IEEE Transactions on Industrial Electronics* 66, no. 1 (2019): 79-89, doi:10.1109/TIE.2018.2821619.
19. Ibtiouen, R., Mezani, S., Touhami, O., Nouali, N. et al., "Application of Lumped Parameters and Finite Element Methods to the Thermal Modeling of an Induction Motor," in *IEMDC 2001. IEEE International Electric Machines and Drives Conference* (Cat. No. 01EX485), Cambridge, MA, 2001, 505-507, doi:10.1109/IEMDC.2001.939354.
20. Idoughi, L., Mininger, X., Bouillault, F., Bernard, L. et al., "Thermal Model with Winding Homogenization and FIT Discretization for Stator Slot," *IEEE Transactions on Magnetics* 47, no. 12 (2011): 4822-4826, doi:10.1109/TMAG.2011.2159013.
21. Hanisch, L.V. and Henke, M., "Lifetime Modelling of Electrical Machines Using the Methodology of Design of Experiments," *SNE-Journal* 31, no. 2 (2021): 95-100, doi:10.11128/sne.31.tn.10568.
22. He, J., Somogyi, C., Strandt, A., and Demerdash, N.A.O., "Diagnosis of Stator Winding Short-Circuit Faults in an Interior Permanent Magnet Synchronous Machine," in *2014 IEEE Energy Conversion Congress and Exposition (ECCE)*, Pittsburgh, PA, 2014, 3125-3130, doi:10.1109/ECCE.2014.6953825.
23. Bonnett, A.H. and Yung, C., "Increased Efficiency versus Increased Reliability," *IEEE Industry Applications Magazine* 14, no. 1 (2008): 29-36, doi:10.1109/MIA.2007.909802.
24. IEC 60172:2020-11, "Test Procedure for the Determination of the Temperature Index of Enamelled and Tape Wrapped Winding Wires," November 2020.

25. IEC 60034-18-21:2012-09, "Rotating Electrical Machines—Part 18-21: Functional Evaluation of Insulation Systems—Test Procedures for Wire-Wound Windings—Thermal Evaluation and Classification," September 2012.
26. Mancinelli, P., Stagnitta, S., and Cavallini, A., "Qualification of Hairpin Motors Insulation for Automotive Applications," *IEEE Transactions on Industry Applications* 53, no. 3 (2017): 3110-3118, doi:10.1109/TIA.2016.2619670.
27. Madonna, V., Giangrande, P., and Galea, M., "Weibull Distribution and Geometrical Size Factor for Evaluating the Thermal Life of Electrical Machines' Insulation," in *IECON 2020 the 46th Annual Conference of the IEEE Industrial Electronics Society*, Singapore, 2020, 1114-1119, doi:10.1109/IECON43393.2020.9255227.
28. Madonna, V., Giangrande, P., and Galea, M., "On Specimens Choice for Thermal Lifetime Assessment of Low Voltage Electrical Machines Insulation," in *The 10th International Conference on Power Electronics, Machines and Drives (PEMD 2020)*, 2020, 38-43, doi:10.1049/icp.2021.1127.
29. Dakin, T.W., "Electrical Insulation Deterioration Treated as a Chemical Rate Phenomenon," *Transactions of the American Institute of Electrical Engineers* 67, no. 1 (1948): 113-122, doi:10.1109/T- AIEE.1948.5059649.
30. Lahoud, N., Nguyen, M.Q., Maussion, P., Malec, D. et al., "Lifetime Model of the Inverter-Fed Motors Secondary Insulation by Using a Design of Experiments," *IEEE Transactions on Dielectrics and Electrical Insulation* 22, no. 6 (2015): 3170-3176, doi:10.1109/TDEI.2015.005202.
31. Talukdar, B.K. and Deka, B.C., "An Approach to Reliability, Availability and Maintainability Analysis of a Plug-In Electric Vehicle," *World Electric Vehicle Journal* 12, no. 1 (2021): 34, doi:10.3390/wevj12010034.